An experimental perspective on the effects of initial structures on rock avalanches' propagation and sedimentary characteristics

Zhao Duan[1,2], Yan-Bin Wu[2,3*], Qing Zhang[2,3], Zhen-Yan Li[2,3], Lin Yuan[2,3], Kai Wang[2,3], Yang Liu[2,3]

[1] Associate Professor, College of Geology and Environment, Xi'an University of Science and Technology, Xi'an, 710054, China

[2] Institute of Ecological Environment Restoration in Mine Areas of West China, Xi'an University of Science and Technology, Xi'an, 710054, China

[3] Graduate Student, College of Geology and Environment, Xi'an University of Science and Technology, Xi'an, 710054, China

*Corresponding to: Yan-Bin Wu (19209071021@stu.xust.edu.cn)

Abstract: Deposit morphologies and sedimentary characteristics are direct threads for investigating rock avalanches. However, these two characteristics and mobility become ambiguous because of the initial discontinuity sets. Therefore, experiments were conducted with different initial configurations of blocks (the long axis of the blocks perpendicularly placed to the strike of the inclined plate EP, parallel to the strike of the inclined plate LV, perpendicular to the inclined plate LP, randomly R and without the blocks NB as a control experiment) and different slope angles in this study. The experimental materials comprised both block and granular materials to simulate large blocks and matrixes, respectively, in natural rock avalanches. The results revealed that the mobility of the mass flows was enhanced at LV, LP and R configurations, whereas it was restricted at the EP configuration. The mobility decreased with the increase in slope angles at LV configurations. Strand protrusion of the blocks made the elevation of the deposits at LV configuration larger than that at EP, LP, and R configurations. An alternate deflection of the blocks for the bending moment that was created during the lateral spread of the mass flows was responsible for creating zigzag structures. Varying degrees of deflection of the blocks demonstrated different levels of collision and friction in the interior of the mass flows; the most intensive collision was observed at EP. In the mass deposits, the blocks' orientation was affected by their initial configurations and the motion process of the mass flows. This research would provide more ideas for investigating rock avalanches' surface morphologies and sedimentary characteristics.

1 Introduction

Rock avalanches are a type of ubiquitous geological phenomenon on the earth's surface. Their motion processes often involve multiple granular materials, ranging from large blocks to tiny particles (Ui et al., 1986; Voight and Pariseau, 1978). Many rock avalanches have large blocks with hypermobility (Dufresne, 2012; Mangeney et al., 2010; Goujon et al., 2003; Phillips et al., 2006; Delannay et al., 2017). In some cases, these huge blocks have a larger runout (Charrière et al., 2016; Schwarzkopf et al., 2005). The deposits of rock avalanches often have particular surface structures, such as transverse ridges and lateral levees

30   (Wang et al., 2019; Shea and Van Wyk De Vries, 2008), and unique sedimentary characteristics, such as the inverse grading of granules (Schwarzkopf et al., 2005; Fisher and Heiken, 1982; Dufresne et al., 2016; Hungr, 2006; Duan et al., 2021) and block orientation (Pánek et al., 2008; Wang et al., 2019). Several factors affect the motion process and sedimentary morphologies of rock avalanches (Manzella and Labiouse, 2009; Phillips et al., 2006; Yang et al., 2011; Duan et al., 2020; Li et al., 2021; Duan et al., 2019). However, the initial structures at the source area and components of a rock avalanche are critical to the study of

35   rock avalanches (Duan et al., 2020; Huang and Liu, 2009; Lucas and Mangeney, 2007; Bartali et al., 2020; Manzella and Labiouse, 2009; Phillips et al., 2006; Manzella and Labiouse, 2013a; Crosta et al., 2017).

Field investigations are one of the fundamental methods for examining rock avalanches. During these investigations, the initial structures and components of the rock mass in the source area, as well as the surface structures and sedimentary characteristics of rock avalanches' deposits, are studied by the researchers. Disaggregated rock masses occurring due to discontinuity sets are

40   observed extensively in the source area of a rock avalanche. Importantly, several small granules are packed in between these discontinuities. Disaggregated rock structures facilitate the occurrence of a rock avalanche. In some recent cases, the rock avalanches with initial structures in their source area exhibited greater mobility, but it is unclear whether their hypermobility is connected to their initial structures.

In previous studies, the deposits of rock avalanches have been extensively investigated to reveal the dynamic characteristics

45   of rock avalanches during motion. For a rock avalanche's deposit, the spatial distribution of particle size (Gray and Hutter, 1997; Zeng et al., 2020; Zhao et al., 2021; Baker et al., 2016; Getahun et al., 2019; Dufresne et al., 2016) and the arrangement of blocks (Pánek et al., 2008; Wang et al., 2019; Moreiras, 2020; Dufresne et al., 2021) are prominent features requiring thorough examinations. In fact, the latter has become a hotspot for investigation. An obvious orientation of the long axis of large blocks (Figure 1) was clearly discerned on the deposits of The Taheman rock avalanche and Nixu rock avalanche in Tibet

50   plateau, China (Wang et al., 2021), the rock avalanche on the Black Rapids Glacier, Alaska (Shugar and Clague, 2011), and the Jiweishan rock avalanche in Chongqing, China (Zhang et al., 2019). For studying the pyroclastic flow deposits that occurred in the NE area of Arequipa, South Peru, Dufresne et al. (2021) quantified the orientation of large blocks using a statistical method. They stated that the compression of deposits caused the orientation during accumulation. It is plausible to believe that the orientation of large blocks is closely related to the mobility process of rock avalanches. However, it is unclear whether the

55   process is related to the initial structures in the source area of rock avalanches.
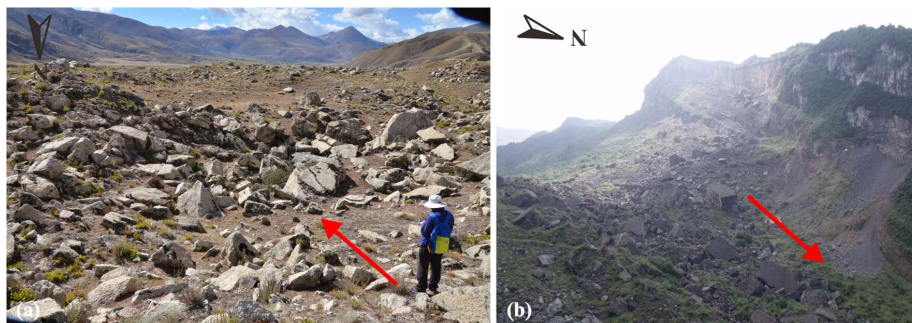
Figure 1: Giant blocks and their orientations (the red arrow indicates the motion direction of the rock avalanches): (a) Nixu rock avalanche in Tibet plateau, China (the base photo was provided from professor Yufeng Wang and Qiangong Cheng (Wang et al., 2021)); (b) Jiweishan rock avalanche in Chongqing, China (the base photo was provided from professor Ming Zhang (Zhang et al., 2019)).

In rock avalanches, it is challenging to systematically obtain the initial fracture structures of original rock and the orientation of large blocks in the deposits by field investigation due to the differences in geological environments. The same is true for their motion processes. Consequently, it is difficult to find a relationship between these rock avalanches' characteristics.

Therefore, physical model experiments, in which the blocks with rectangular shapes were poured into a container either regularly or randomly, were established to study the dynamical characteristics and deposit morphologies of rock avalanches (Manzella and Labiouse, 2009; Phillips et al., 2006; Yang et al., 2011; Manzella and Labiouse, 2013a). Manzella and Labiouse (2009) illustrated that the runout of experimental rock avalanches was larger when the long axis of the blocks was adjusted parallelly to the strike of the inclined plate than that when the blocks were filled randomly. Bowman and Take (2015) also performed model experiments and used different initial configurations of large blocks to examine the mobility of rock avalanches. However, it was noted that the conditions that cause the long axis of blocks pointing toward other directions were absent in their experiments. In addition, for natural rock avalanches, the material components include both large blocks and matrixes with smaller particle sizes (Glicken, 1996), whereas the materials used in aforesaid experimental studies were totally large blocks or granules with small particle sizes. Yang et al. (2011) conducted experiments on the materials comprising simultaneously large blocks and granular matrixes. However, the blocks were cubes; therefore, the researchers could not examine the orientation characteristics of large blocks in deposits. Experiments combining large blocks and granular matrixes were also conducted by Phillips et al. (2006). Based on the experimental results, they clearly interpreted the reasons for hypermobility in the rock avalanches. Nonetheless, they discussed briefly about the deposit morphologies and sedimentary characteristics.

The abovementioned experimental studies can provide a firm foundation for the dynamics of rock avalanches. Nevertheless, experiments on the materials comprising both large blocks and granular matrixes should be conducted to study the mobility and deposit morphologies of rock avalanches at different initial structures of the original rock. Moreover, the influencing factors and possible reasons for the long axis orientation of large blocks in rock avalanches' deposits should be probed from

experimental viewpoints.

Hence, physical model experiments with materials containing large blocks and granular matrixes were performed in this study.

85   The large blocks were set with different initial structures to simulate rock avalanches with a rock mass disaggregated by discontinuity sets to examine the motion process, surface structures and sedimentary characteristics of rock avalanches. The objectives of this study are: (1) to examine the changing ~~lows of the~~ mobility of rock avalanches at different block configurations and slope angles; (2) to explore the differences and reasons for the surface structures and sedimentary characteristics of deposits under those two factors; and (3) to determine the orientation of large blocks' long axis in each

90   experimental rock avalanche's deposit and interpret the orientation differences from their motion processes. This research may provide a reference for investigating the mobility of rock avalanches and revealing the reason for large blocks' orientation.
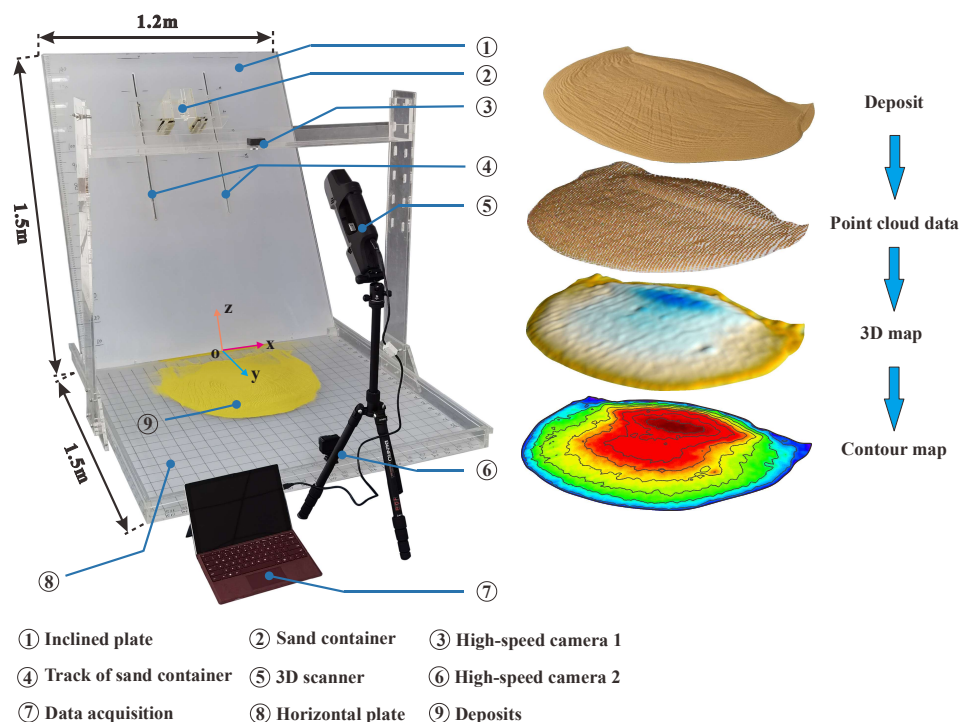
2 Experimental design

2.1 Apparatus

The motion mechanism and deposit morphology of experimental rock avalanches were studied in a sandbox experiment.

95   Plexiglass comprising five parts, namely an inclined plate, a horizontal plate, a sand container, a 3D scanner, and two high-speed cameras, was used to construct the experimental devices. A pair of sandbox tracks were installed in the inclined plate to adjust the sandbox's height. The horizontal and inclined plates were 1.5 m long and 1.2 m wide, respectively (Fig. 2). The specified volume of the sandbox with a side-by-side gate was $3.6 \times 10^{-3}\,\mathrm{m^3}$. A 3D scanner (8 frames/s, 1.3-megapixel resolution) captured the whole process of the experimental rock avalanches in motion and generated 3D coordinate data of the free surface.

100   The accuracy of the 3D scanner was 0.1 mm. It had three lenses: an emitter lens at the bottom and two lenses at the top—one with a near-infrared (NIR) sensor and one that could acquire colour images. During scanning, an NIR ray was emitted, reflected from the objects' surfaces, and received by the lenses at the top of the 3D scanner. The received NIR data were converted into 3D cloud data and colour images. The 3D data were collected according to the principles of stereoscopic parallax and active triangular ranging. Two high-speed cameras (120 frames/s, 0.4-megapixel resolution) were used to collect images at the end

105   of each experiment. One was placed on a camera shelf, which could be adjusted up and down and front to back, to obtain deposit photos with a bird view. The other one was fixed at the front of the horizontal plate with a front view.

Figure 2: Experimental apparatus.

① Inclined plate	② Sand container	③ High-speed camera 1
④ Track of sand container	⑤ 3D scanner	⑥ High-speed camera 2
⑦ Data acquisition	⑧ Horizontal plate	⑨ Deposits

2.2 Materials

110   The cuboid blocks (Fig. 3 (a)) were manufactured from quartz sand and cemented with epoxy glue to simulate the large blocks in natural rock avalanches. These cuboid blocks had a mass of 38 ± 0.1 g and specifications of $20 \times 20 \times 40$ mm. The corresponding equivalent particle size was 31.26 mm.

The quartz sand (Fig. 3(b)) simulated the granular matrixes filled into between the blocks. Figure 4 depicts the particle size distribution of the sand. It had an uneven coefficient C_u of 2.39, a curvature coefficient C_c of 1.19, an average diameter of 0.2

115   mm and a specific surface area of 0.02 m²·kg⁻⁴. The cumulative percentage of particles in size range of 0.075–0.42 mm was 87.71%, the average particle size was 0.18 mm, the internal friction angle φ was 36°, the cohesion c was 0, and the interface friction parameter of plexiglass and sand was 0.42.

The ratio between the equivalent particle size of the blocks and the average particle size of the sand was 156:1. This ratio was between 167:1 and 45:1, which is the ratio interval of equivalent particle size between large blocks and granular matrixes for

120   natural rock avalanches (Dufresne et al., 2016). The mass ratio between the epoxy glue and sand was 1:3.
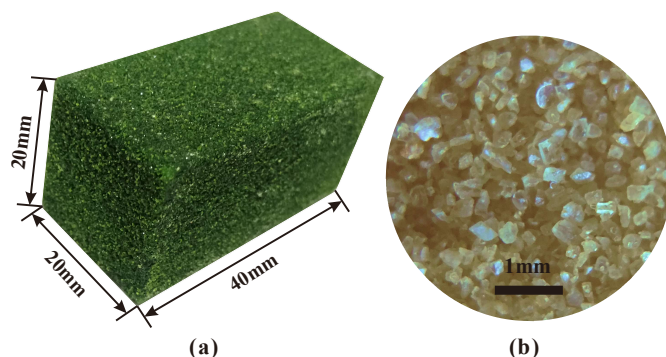
Figure 3: Experimental material: (a) cuboid block made of green quartz sand; (b) quartz sand.
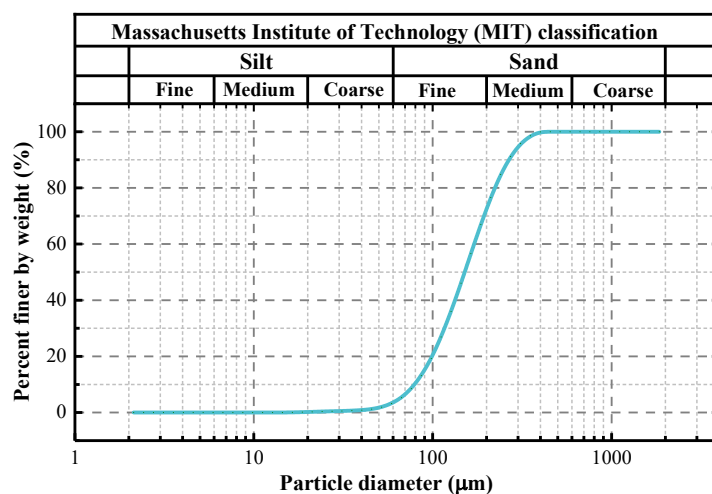

Figure 4: Particle size distribution of experimental material.

2.3 Experimental method

Figure 5 shows the deposit morphologies of experimental rock avalanches. The blocks are placed in four kinds of configurations when they are filled into the sand container: the long axis of the blocks perpendicular to the strike of the inclined plate (EP), parallel to the strike of the inclined plate (LV), perpendicular to the inclined plate (LP), and randomly (R). In addition, a contrast experiment without blocks (NB) was also designed in this study. Figure 6 shows the variation of block configurations and slope angles. Except for the contrast experiment, the percentage of blocks was 25% for each experiment group, which was between 10% and 80% for natural rock avalanches (Makris et al., 2020; Dufresne and Dunning, 2017; Dufresne et al., 2016). Manzella and Labiouse (2009) revealed that the rock avalanche exhibited greater mobility at the LV configuration. Hence, experiments were also conducted at 40°, 50°, 60° and 70° with LV configuration to explore the effects of slope angles. Table 1 presents the details of the experimental scheme. The height of the centre of gravity for each group of the experiments was 0.7 m. The volume of the sand container was $3.6 \times 10^{-3}\,\text{m}^3$.

While preparing for the experiments, the inner surface of the sand container and the inclined and horizontal plates were

cleansed with static-proof liquid. After drying these cleaned apparatuses, the sand of 180 g was poured in and levelled.

Thereafter, 12 blocks were arranged on the even sand layer, and a third layer of sand of 180 g was then poured in to cover the

first 12 blocks and levelled. The abovementioned filling procedures were repeated thrice till the sand container was filled

140   completely. After the filling operations were completed, the sand container's gate was opened and the whole mobility process

of an experimental rock avalanche was captured using a 3D scanner and two high-speed cameras.

The friction coefficient of the interface between sand and the plexiglass must be obtained. The direct shear tests were performed

to determine the internal friction angle of the interface, and the tangent value of the internal friction angle was used as its

friction coefficient. During the tests, a customised plexiglass cylinder φ61.8×10 mm was installed into the lower shear box.

145   The sand or blocks had the exact specification as the customised plexiglass cylinder and was filled into the upper shear box.

Therefore, the shear surface is the interface (Figure 7).

Table 1 Experimental scheme

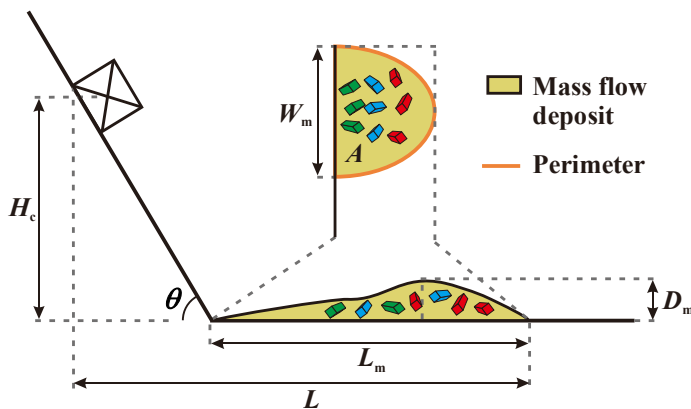| Experimental numbering	Block configuration	Slope angle (°)	Gravity height (m)	Matrix density (10^3kg·m^{-3})	Block amount	Matrix volume in the sand container (10^{-6}m)
EP-50	EP	50	0.7	1.5	36	2.904
LV-50	LV	50	0.7	1.5	36	2.904
LP-50	LP	50	0.7	1.5	36	2.904
R-50	R	50	0.7	1.5	36	2.904
NB-50	NB	50	0.7	1.5	0	3.6
LV-40	LV	40	0.7	1.5	36	2.904
LV-60	LV	60	0.7	1.5	36	2.904
LV-70	LV	70	0.7	1.5	36	2.904

150   **Figure 5: Diagram of experimental rock avalanches: L_m = Maximum length of the deposit; W_m = maximum width of the deposit; D_m = maximum depth of the deposit; A = area of the deposit projected on the horizontal plane; P = perimeter of the deposit; θ = slope angle; H_c = height of the sandbox from the centre of gravity; and L = Runout of the sliding mass.**
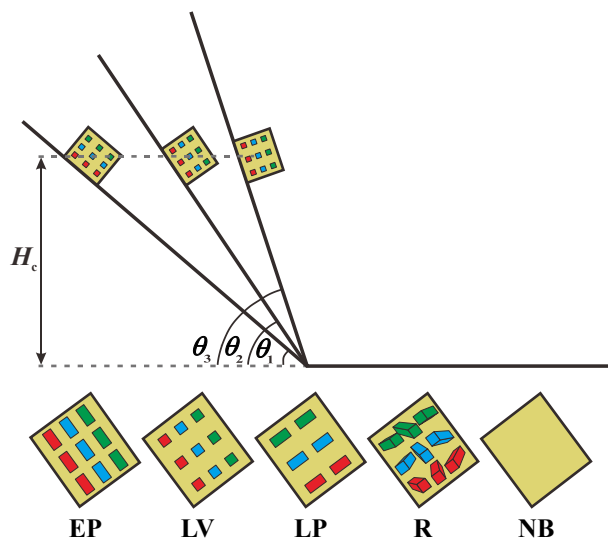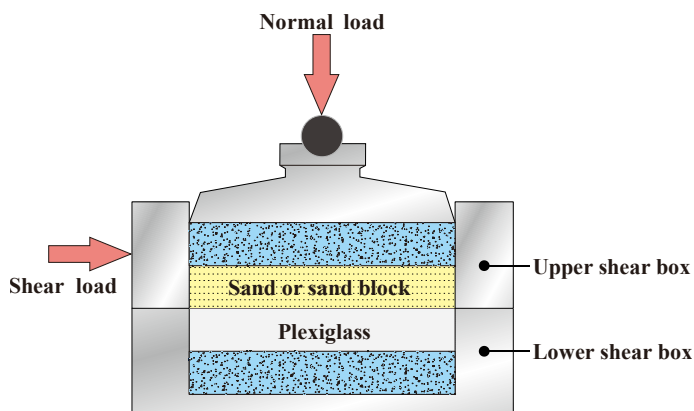
Figure 6: Variable sets of the experiments.

Figure 7: Diagram of direct shear tests at sand-plexiglass interface.

3 Results

3.1 Runout and velocity

Figure 8 demonstrates the runout of each experimental rock avalanche. At different block configurations, the runout of experimental rock avalanches had a minimum value of 114.81 cm at EP-50 and a maximum value of 128.33 cm at R-50. Notably, the runout at the EP-50 configuration was smaller than that at NB-50 configuration (116.89 cm). At the LV configuration, the runout decreased linearly with the increase in the slope angles.
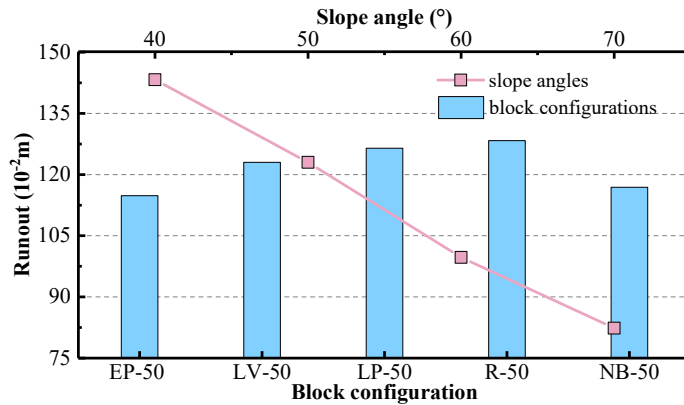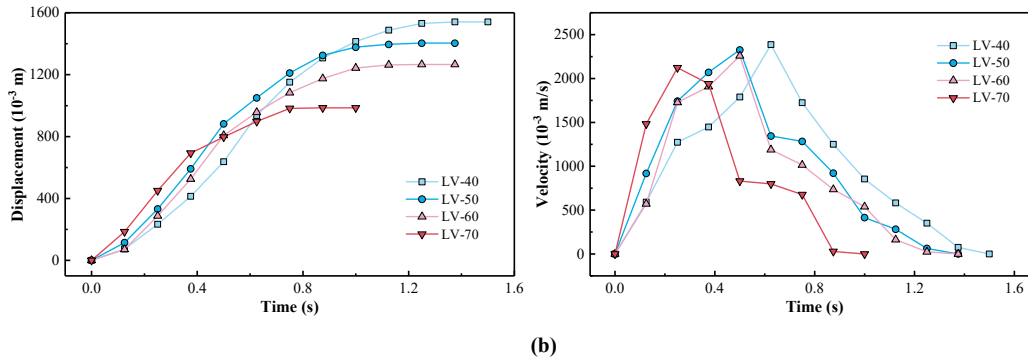
Figure 8: The runout of the experimental rock avalanches.

<mark>The displacement of experimental rock avalanches was defined as the difference between the front position of the mass flow and the starting point, which was present at the bottom of the overlap surface (displacement = 0) between the sand container and the inclined plate.</mark> Figure 9(a) shows that the <mark>duration</mark> of the mass flows was 1.375 s at EP-50, LV-50, LP-50, and NB-50, but was 1.5 s at R-50. The displacement showed an exponentially increasing trend at the early stage, then a logarithmically increasing trend at the later stage. The peak velocity of the mass flows was approximately 2300×10^{-3} m/s at LV-50, LP-50, R-50, and NB-50, but was 2016×10^{-3} m/s at EP-50, which was apparently smaller than those four conditions. The point of time was 0.5 s when these five mass flows reached their peak velocities.

Figure 9(b) illustrates that the duration of the mass flows decreased with the increase in slope angles. The durations at LV-40, LV-50, LV-60, and LV-70 were 1.5 s, 1.375 s, 1.375 s, and 1 s, respectively. The displacement of the mass flows at different slope angles demonstrated the same trend as those at different block configurations. With the increase in slope angles, the peak velocity of the mass flows and the time they spent to reach their peak velocity were decreased. The front of the mass flows reached the slope break at the same time at which the mass flows attained their peak velocity.
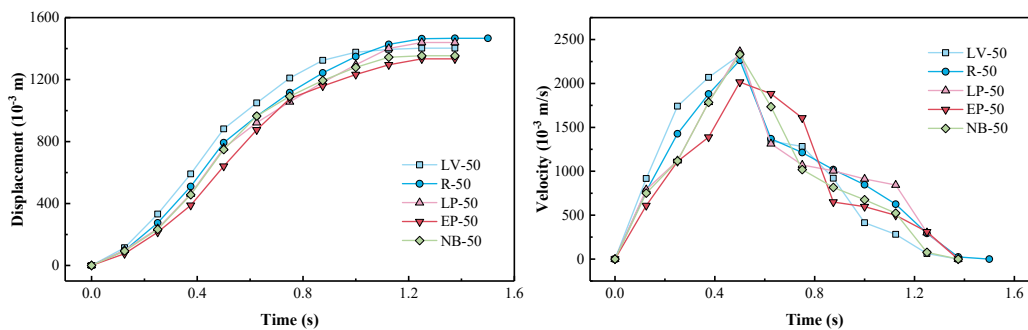
(a)

180

Figure 9: Dynamic characteristics of the experimental rock avalanches: (a) at different block configurations; (b) at different slope angles.

3.2 Morphology of deposits

185   **3.2.1 Morphological parameters**

Figure 10(a) shows the maximum length of the deposits of the mass flows. The histogram of Figure 10(a) shows that the length had a maximum value of 647.76 mm at R-50 but had a minimum value of 512.5 mm at EP-50, which was smaller than the value at NB-50. The line chart of Figure 10(a) revealed that the length increased first and then decreased with the increase in slope angles. It attained a maximum value of 669.83 mm at LV-50.

190   The histogram of Figure 10(b) shows that the width had a maximum value of 781.86 mm at R-50 but had a minimum value of 703.29 mm at LP-50. The deposit width at EP-50, LV-50, and LP-50 was smaller than the width at NB-50. The line chart of Figure 10(b) shows that the width increased first and then decreased with the increase in slope angles.

The histogram of Figure 10(c) shows that the depth had a maximum value of 41.42 mm at LV-50 but had a minimum value of 33.42 mm at R-50. The depth at EP-50 and R-50 was smaller than the width at NB-50. The line chart of Figure 10(c) shows

195   that the width decreased first but increased at 60°.

The histogram of Figure 10(d) shows that the deposit area had a maximum value of $3495.67 \times 10^{-6}\,\text{m}^2$ at R-50 and a minimum value of $2485.6 \times 10^{-6}\,\text{m}^2$ at EP-50. The line chart of Figure 10(d) shows that the area increased first and then decreased with the increase in slope angles.

The histogram of Figure 10(e) shows that the perimeter–area ratio had a maximum value of 0.089 at EP-50 but had a minimum

200   value of 0.071 at LV-50. The line chart of Figure 10(e) shows that the perimeter–area ratio had a maximum value of 0.089 at LV-60; however, it was smaller than that at EP-50.

A comparison showed that the block configurations exerted a more significant effect on the deposit parameters of the mass flows than slope angles. These deposit parameters had a larger amplitude of variation at different block configurations.

(a)

(b)

(c)

(d)

(e)
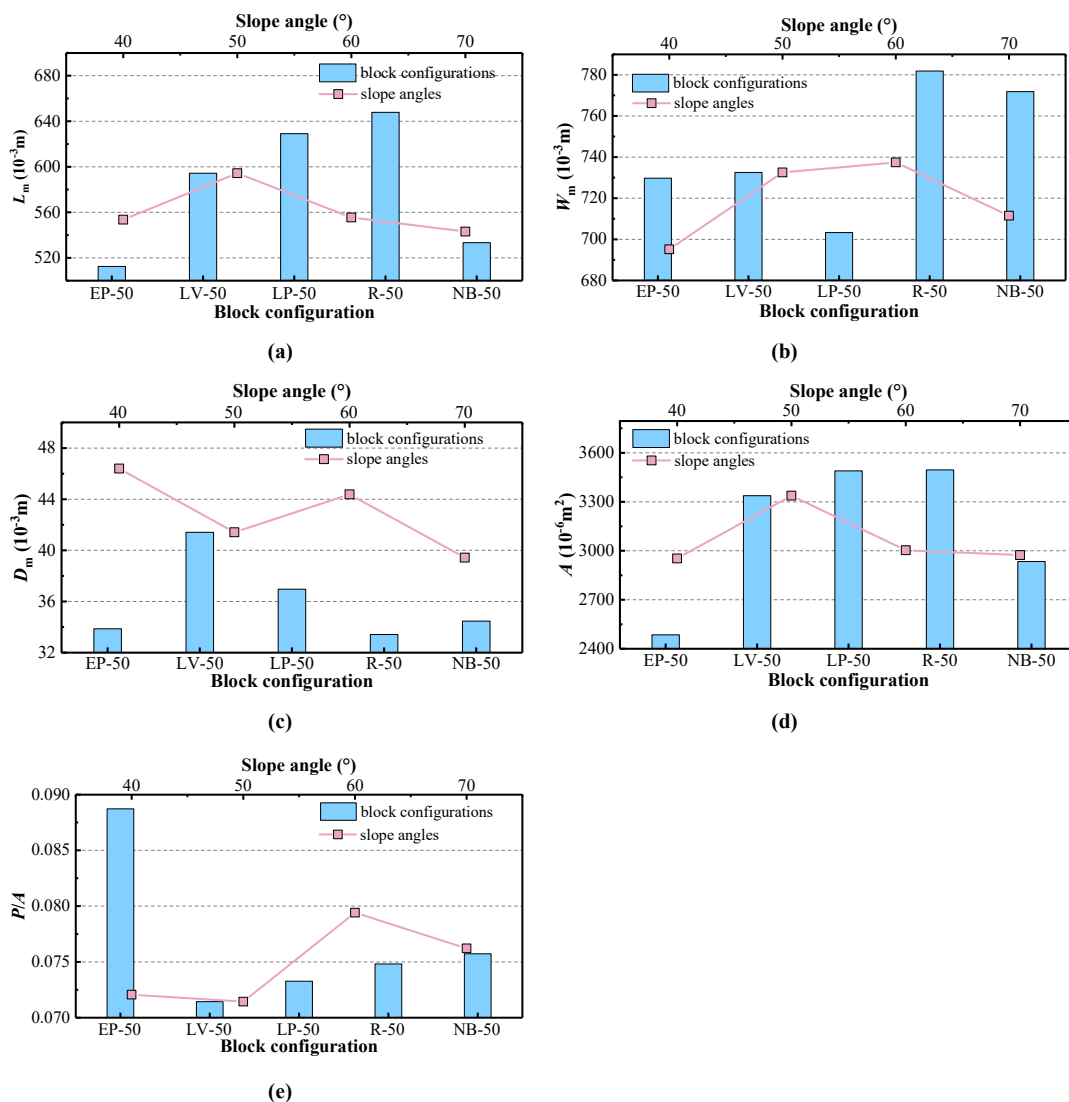
Figure 10: Deposit morphology parameters of the experimental rock avalanches: (a) the maximum length ~~with block configuration and slope angle~~; (b) the maximum width ~~with block configuration and slope angle~~; (c) the maximum depth ~~with block configuration and slope angle~~; (d) the area ~~with block configuration and slope angle~~; and (e) the perimeter–area ratio ~~with block configuration and slope angle~~.

3.2.2 Surface structures and sedimentary characteristics

The data elevation model of the mass deposits can be established using the point cloud data obtained by the 3D scanner. This model can reflect the elevation characteristics of the deposits (Figure 11(a)) under the impact of block configurations and slope angles. A thorough comparison reveals that the elevation of the mass flows at EP-50, LP-50, R-50, and NB-50 was apparently smaller than that at LV-40, LV-50, LV-60, and LV-70. At EP-50, LP-50, and R-50, the surface elevation was similar to NB-50. Moreover, no apparent protrusion of blocks was visible on the deposit surface (Figure 11(a)), demonstrating that no apparent

11

220   separation of the blocks and the granular matrixes was present. At LV-40, LV-50, LV-60 and LV-70, the elevation of granular

matrixes was approximately equal to the elevation of the deposits at EP-50, LP-50, R-50, and NB-50. A string of protrusions

was observed on the surface of the deposits (Figure 11(a)). Figure 11(b) shows the protrusion of the stranding blocks. At LV-

40 and LV-50, some blocks were located away from the main deposit at a different position.
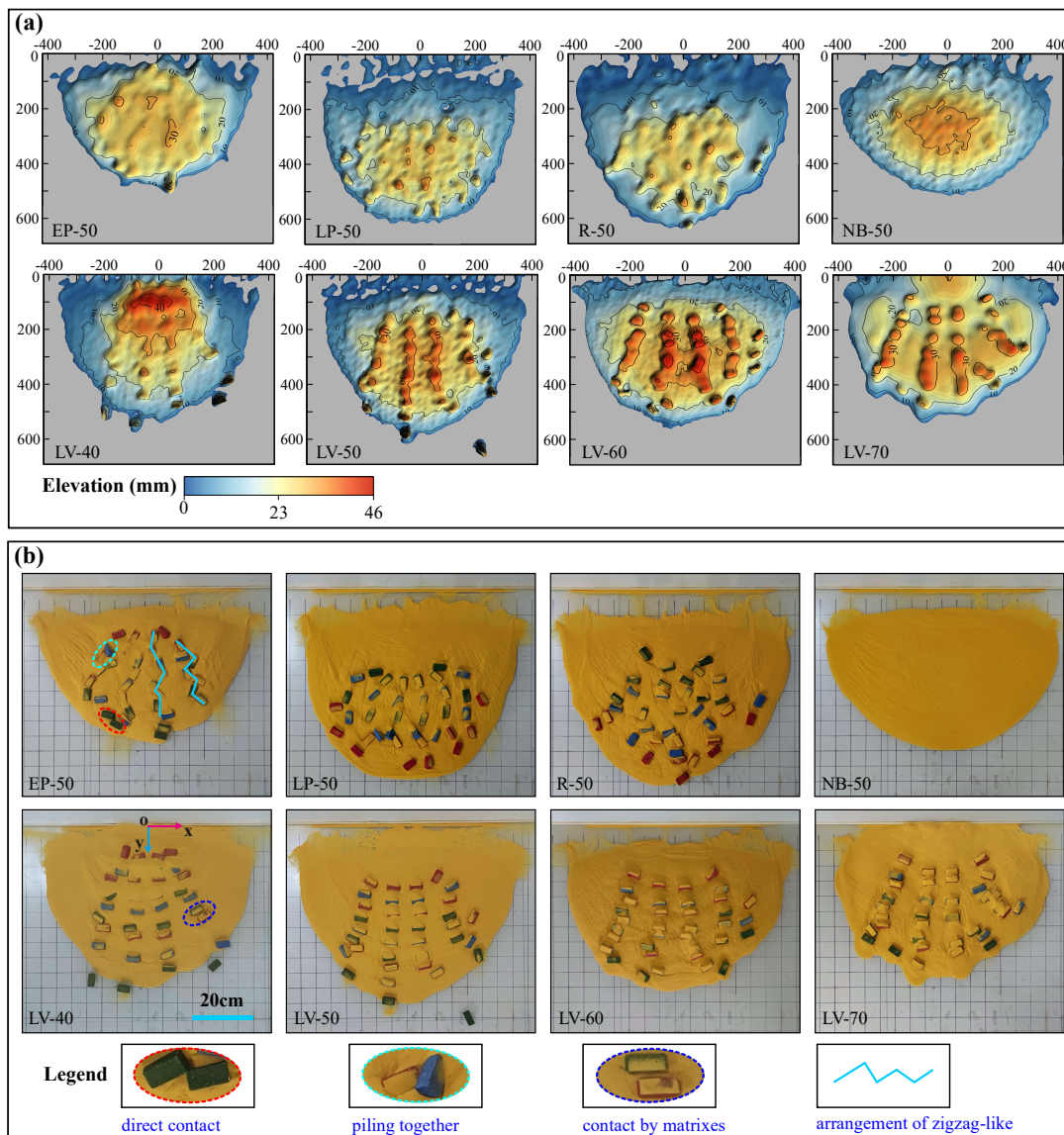
Figure 11: The surface morphology of the rock avalanches' deposit: (a) contour maps with elevation; (b) images of these
rock avalanches.

Figure 11 (b) present the direct contact relationship and arranging characteristics of the mass deposits. At EP-50 and LP-50,

the symmetry of the deposits and their inner blocks was relatively low along the y-axis. The spacing between blocks was small.

Several contact ways, such as direct contact, contact by matrixes and piling together, were discerned in the mass deposits. The

230   blocks formed a series of zigzag-like structures on the deposit surfaces at EP-50 and LP-50. At R-50, the blocks in the deposit

exhibited no symmetry. Direct contact and contact by matrixes were just two kinds of contact ways. Furthermore, the structures

of piling together were absent.

At LV-40, LV-50, LV-60 and LV-70, the deposits and their inner blocks showed good symmetry along the *y*-axis. The long axis

of the blocks closed to the *y*-axis had a small angle along the *x*-axis; however, the angle grew larger with the increase in the

235   distance between the blocks and the *y*-axis. In these four conditions, the blocks came into contact through matrixes. In addition,

the matrixes covered on the surface of the blocks increased by comparing with those at EP-50, LP-50, and R-50.

3.3 Orientation of blocks in deposits

In this study, the direction of the long axis of the blocks was counted to quantitively examine the orientation of the blocks in

the mass deposits. The *y*-axis was defined as 0° during the statistical analysis; based on this, the orientation of the blocks was

240   obtained. Figure 12 shows that the blocks still exhibited predominant orientations for each group of experiments despite having

a distribution of multiple orientations at EP-50, LP-50, and R-50. The orientation of the blocks at EP-50 was mainly towards

20°, 70°, 130°, and 150°. At LP-50, the orientation of the blocks was mainly at intervals of 310°–360° and 0°–10°. At R-50,

the orientation of the blocks occurred mainly at 80° and 120°.

At LV-40, LV-50, LV-60 and LV-70, the long axis of the blocks arranged towards a uniform direction increased compared with

245   that at EP-50, LP-50, and R-50. At LV-40, LV-50, LV-60 and LV-70, the orientation of the blocks was mainly observed between

60° and 90°, but a distribution of 40° and 120° was still observed at LV-70.
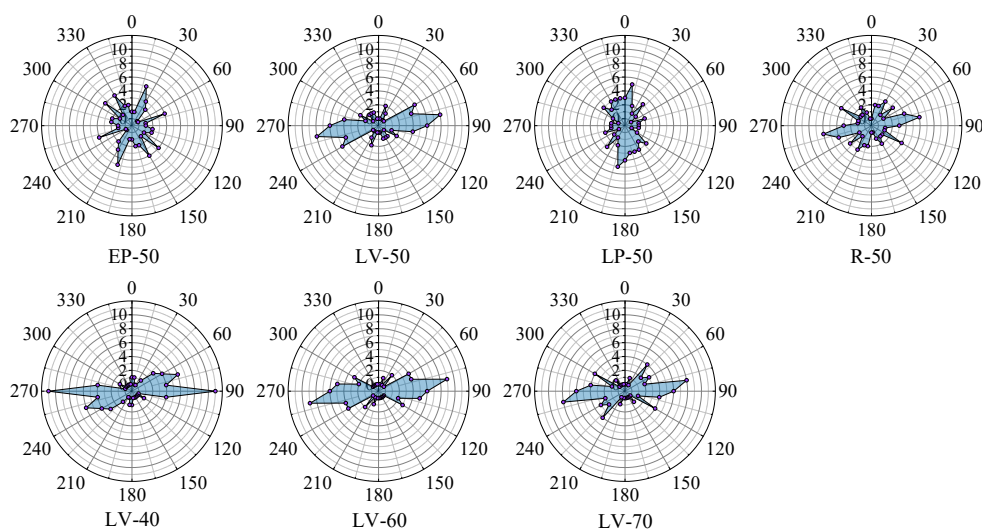
Figure 12: The orientation of the blocks in the deposit of the experimental rock avalanches.

4 Discussions

250 **4.1 Runout of experimental rock avalanches**

The blocks' configuration at the source area exerted a significant influence in the runout of rock avalanches. The runout of the mass flow was largest at R-50, which was attributed to the release of the blocks. These blocks were randomly stacked in the container. Following the release of materials, the blocks stacked at a higher position would lower their centre of gravity due to an unstable piling state. As a result, they push the front mass forward, resulting in the mass flow having a maximum runout

255 and the depth and height of the centre of gravity of the deposits having minimum values. For LV-50, the energy dissipation caused by collision and friction during motion decreased because of a regular arrangement of the blocks. Nonetheless, the deposit showed a high level of the centre of gravity, meaning that the mass flow had high potential energy at the end of the motion. Hence, the kinetic energy transformed from the potential energy of the mass flow was comparatively low. Correspondingly, the runout of the mass flow was smaller than the runout at R-50. At EP-50, the long axis of the blocks was

260 present along the direction of the mass flow before its release; therefore, the lateral spreading of the mass flow during motion would change the direction of the blocks to a larger extent. During the motion, the energy of the mass flow dissipated by collision and friction among the blocks was larger; hence, its runout was minimum. The closing contact and change in the blocks' orientation offered direct evidence that a dramatic interaction of the blocks occurred during the motion. At LP-50, the blocks were perpendicular to the inclined plate before the release, in which they would evolve to the form of EP-50 gradually

265 during the motion and transfer more energy to the front mass. However, the energy loss due to collision and friction of the blocks decreased compared with EP-50. Therefore, the mass flow had a relatively longer runout.

Slope angles also have a noticeable impact on the runout of mass flows. The results demonstrated that the runout was decreased with the increase in the slope angles, which was consistent with previous studies (Fan et al., 2016; Crosta et al., 2015; Crosta et al., 2017; Duan et al., 2020), regardless of the experimental apparatus (with or without side walls). The decreased runout

270 was caused by the energy dissipated from the colliding at the slope break increased with the increase of the slope angles (Zhang et al., 2015; Ji et al., 2019; Wang et al., 2018).

The existence of matrixes also affects the runout of the mass flows. Manzella and Labiouse (2009) showed a converse trend in the same block configurations of LV and R, which was mainly caused by the difference in experimental materials. Because the matrixes were missing from their block studies, the blocks would collide directly and generate friction throughout the

275 motion. Many interlock structures were formed when the blocks were poured into the container. After releasing the mass, the constraints from the container disappeared. Then, the blocks would overcome the interlock structures, and collide and produce friction. This action causes a large amount of energy dissipation during the motion. Moreover, the mass flow had a low runout. At a regular piling of the blocks in Manzella and Labiouse (2009), similar to the configuration of LV in this study, the collision and friction of the blocks decreased dramatically, leading to a large runout of the mass flow. In general, the matrixes served as

14

280   a conduit for transferring the interaction force between blocks to prevent a ~~dramatic~~ direct contact. Because of the matrixes, most of the blocks were in direct contact with each other, and the friction was changed to rolling friction from sliding friction.

4.2 Morphological differences and corresponding reasons

The protrusion of blocks in the deposit at the LV configuration was clearly distinct from those at the other configurations. At EP-50, LP-50, and R-50, the deposit surface was at a low elevation, which was attributed mainly to the low thickness of the

285   matrixes beneath the blocks. The thickness was approximately 10 mm and even close to 0 mm somewhere between the deposits. At LV configuration, the thickness of the matrixes beneath the blocks was larger than 10 mm and even close to 20 mm in somewhere between the deposits. The protrusion of large blocks was often observed on the deposit surface of natural rock avalanches (Shugar and Clague, 2011; Cole et al., 2002; Schwarzkopf et al., 2005). The process for protrusion because of the stranding of large blocks was similar to that process in which the granular materials generated the inverse grading of particles

290   (large particles sitting at a higher position) under the influence of dispersive pressure and dynamic sieving (Dasgupta and Manna, 2011; Felix and Thomas, 2004).

The regular arrangement and reduced direct contact of the blocks in the deposits at LV-40, LV-50, LV-60, and LV-70 led to the understanding that the blocks might maintain their original arrangement throughout the mobility process at the LV configurations, preventing direct collision and friction. In fact, the blocks tended to keep their initial arrangement from the

295   structure of a regular piling of the blocks in the deposit at an initial LV configuration (Manzella and Labiouse, 2013b).

In this paper, the collision and friction of the blocks during motion were relatively drastic at EP-50, LP-50, and R-50, especially at EP-50, because there were many direct contacts piling structures of the blocks in the deposit (Figure 11(b)). The blocks would deflect throughout the motion, causing the matrixes surrounding them to be pushed aside and allowing the blocks to immerse into the area. As a result, the thickness of the matrixes beneath the blocks was smaller at EP-50, LP-50, and R-50.

300   Correspondingly, the depth of these deposits was smaller.

The zigzag structure comprising a string of blocks is a type of unique phenomenon occurring on the deposit surface. Phillips et al. (2006) have also produced similar results. In their study, the rectangular glass slabs were arranged with their long axis vertical and their largest face parallel to the plane of the gate, similar to the configuration in which the rectangular sand blocks were placed parallel with the inclined plate and vertical to its dip. The zigzag structures were also observed in their experiments.

305   The reason for their formation was unknown. Figure 13 shows the process for the formation of the zigzag structures in this study. Because there were no sidewalls in the path of the mass flows, they would spread laterally, subjecting the backside of a block subject to a force F_1 at an angle with the y-axis. The force can be divided into F_{1x} and F_{1y} along the x-axis and y-axis, respectively. The F_{1y} would push the block forward, whereas F_{1x} would generate a bending moment clockwise. the block deflected is under the influence of the bending moment. Meanwhile, the matrixes on the front side of the blocks would be

310   subjected to a force F_{2x} along the negative x-axis, making the blue block on the front of the red block face a bending moment

M_2 and consequently deflect counterclockwise. By parity of reasoning, the front blocks would deflect clockwise and counterclockwise. As a result, the zigzag structure was formed during this process.
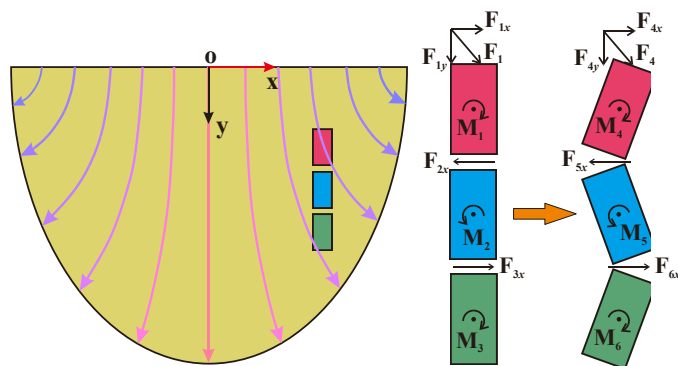
Figure 13: The formation of zigzag arrangement of the blocks. The streamlines with a gradient colour depict the lateral
315   **spreading of a mass flow.**

4.3 Orientation of blocks

Naturally, the orientation of large blocks is observed in the deposit rock avalanches (Mcdougall, 2016; Fisher and Heiken, 1982; Zhang et al., 2019; Pánek et al., 2008; Dufresne et al., 2021; Deganutti, 2008; Reznichenko et al., 2011; Jomelli and Bertran, 2001; Dufresne, 2017; Shugar and Clague, 2011). Most researchers investigate this phenomenon through field
320   investigation, and they conclude that the phenomenon is closely related to the motion process of rock avalanches. However, it has been unclear how to determine the relationship between the orientation of blocks in deposit and the motion process under different conditions because the geological environments are different for each rock avalanche. Therefore, seven groups of experiments were conducted at different initial configurations of materials to investigate the orientation of the blocks.

Under EP-50, LP-50, and R-50, the long axis of the blocks was multi-orientation, but there were still predominant orientations
325   for each group of the experiments. The existence of predominant orientation at R-50 demonstrated that the variation of orientation of the blocks, which was due to the interaction of the blocks and matrixes, was from disorder to orderly. At EP-50 and LP-50, the unconcentrated orientation of the blocks in the deposit demonstrated a more intensive interaction in interior of the mass flows during the motion because of the lateral spread (Johnson et al., 2012; Mangold et al., 2010; Reznichenko et al., 2011). In these two configurations, the blocks were prone to be affected by the lateral spread because their long axis was along
330   the motion direction of the mass flows. Therefore, the side force due to lateral spread can easily change the blocks' orientation. A more unconcentrated orientation of the blocks at EP-50 comparing with LP-50 demonstrated a more intensive interaction of collision and friction in the mass flow. At EP-50, LP-50, and R-50, the sides of the blocks were buried almost totally and the contact area between the blocks and the matrixes became large. Hence, the force of the blocks from the matrixes was large and correspondingly, leading to a larger number of deflected blocks.

335   At LV configuration, parts of the sides of the blocks were buried by the matrixes. Correspondingly, there was a limited contact

area between the blocks and the matrixes. Therefore, the force of the blocks from the matrixes was small, correspondingly leading to a small deflection of the blocks. The blocks could keep their initial direction well during motion from the approximate direction of 90° of the blocks in the deposits at the initial configurations of LV. With the increase in slope angles, the extent to which the blocks had a similar orientation decreased. At LV-40, the predominant orientation of the blocks was

340   almost 90°, whereas it had a small deflection and some sub-predominant orientation at LV-50, LV-60, and LV-70. The reason was the impact force increased with the increase in the slope angles (Ji et al., 2019; Asteriou et al., 2012; Li et al., 2015). In summary, the orientation of the blocks in the deposits was less influenced by slope angles at the initial configurations of LV.

4.4 Interaction of blocks and matrix

The matrixes perform various functions during the motion of the mass flows. First, the matrixes serve as a medium during the

345   movement of the blocks (Figure 14(a)). The matrixes beneath the blocks reduced the resistance of the blocks while moving forward because they exhibit a rolling characteristic. In the absence of matrixes, the blocks would slide forward. Second, the matrixes changed the interaction form of the blocks during motion (Figure 14(b)). The presence of the matrixes made the interaction of the blocks change from sliding friction to rolling friction. The matrixes made the contact of the blocks flexible and, hence, easily have rotation and variation in position. Third, the matrixes played a buffering role in the blocks at the slope

350   break (Figure 14(c)). The matrixes would fill the slope break and make it a smooth transition from a sharp transition, which led to a gentle process when the blocks get from the inclined plate to the horizontal plate. Therefore, the extent of a change in the orientation of the blocks decreased a lot at the slope break. If the matrixes were absent, the orientation of the blocks would change a lot because of the randomness of the blocks after a colliding at the slope break. That was clearly shown in the experiments of Manzella and Labiouse (2013a). Even at LV configuration, in which the blocks tended to keep their initial

355   orientation, the orientation of the blocks changed a lot because of a collision at the slope break. Fourth, the matrixes exerted a constraining effect on the blocks (Figure 14(d)). The matrixes at the flanks and front of the mass flows would restrict and avoid the separation of the blocks near the boundary during the motion of the mass flows. In the middle part of the mass flows, the matrixes around the blocks limited the change in position and avoided a substantial deflection of the blocks.
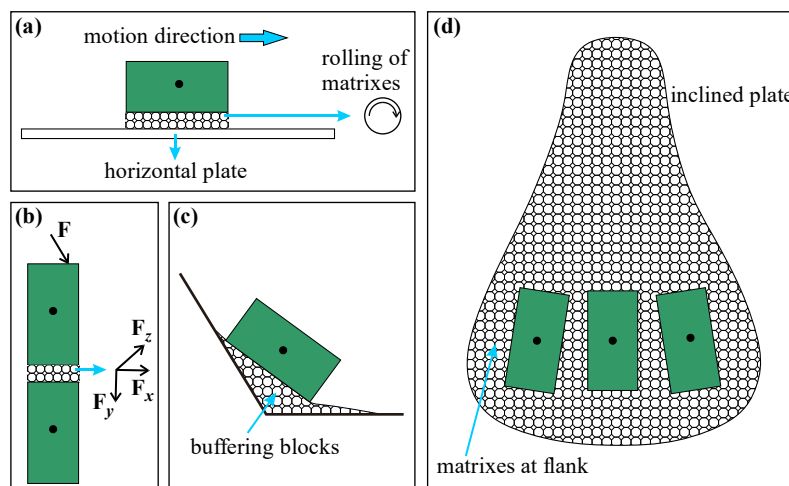
Figure 14: The functions of matrixes in experimental rock avalanches.

To summarise, the matrixes were crucial during the motion of a mass flow. They can avoid a significant change in the blocks'
orientation, act as a buffer for the movement of the blocks to the slope break, and change the friction form of the blocks. In
this paper, the matrixes are medium-fine sand. As a result, they were used to simulate rock avalanches containing both
disaggregated rocks and granular matrixes. However, for some rock avalanches, the matrixes are cohesive; therefore, the
experiments considering different types of matrixes are also worth more studying.

5 Conclusions

(1) The runout of the mass flows varied at different configurations of the blocks. At the initial LV-50, LP-50, and R-50
configurations, the runout of the mass flows was facilitated, which was larger than that at NB-50, but not at EP-50. The runout
decreased with the increase in slope angles.

(2) The elevation of the deposits at configurations of LV was apparently higher than that at EP-50, LP-50, and R-50 due to the
strand protrusion of the blocks. The zigzag structures were caused by an alternate deflection of the blocks for the bending
moment that was generated during the lateral spread of the mass flows.

(3) At the initial EP configuration, the collision and friction in the mass flow were relatively most intensive according to the
small runout, numerous direct contacts of blocks and piling structures. The orientation of the blocks was affected by both the
initial configurations of mass flows and their mobility process. The motion process of the mass flow showed a tendency that
made the orientation of the blocks orderly from disorder in terms of the result of R configuration.

This paper's results would provide threads for studying natural rock avalanches' mobility, surface structures and sedimentary
characteristics. The presence of matrixes in Tock avalanches disaggregated by initial discontinuity sets and subjected to
extensive weathering will be particularly useful in further evaluation.

Availability of data and material

380

The data used to support the findings of this study are included in this paper.

Author contributions

Each author contributed to different parts, here listed: Conceptualisation: Zhao Duan and Yan-Bin Wu, Funding acquisition:

Zhao Duan, Conducting experiments and analysis: Zhao Duan, Yan-Bin Wu, Qing Zhang, Zhen-Yan Li, Lin Yuan, Kai Wang,

385   and Yang Liu; Writing: Zhao Duan, Yan-Bin Wu.

Conflicts of interest

The authors declare that they have no known competing financial interests or personal relationships that could have appeared

to influence the work reported in this paper.

References:

395   Asteriou, P., Saroglou, H., and Tsiambaos, G.: Geotechnical and kinematic parameters affecting the coefficients of restitution

for rock fall analysis, International Journal of Rock Mechanics & Mining Sciences, 54, 103-113,

10.1016/j.ijrmms.2012.05.029, 2012.

Baker, J., Gray, N., and Kokelaar, P.: Particle Size-Segregation and Spontaneous Levee Formation in Geophysical Granular

Flows, International Journal of Erosion Control Engineering, 9, 174-178, 10.13101/ijece.9.174, 2016.

400   Bartali, R., Rodríguez Liñán, G. M., Torres-Cisneros, L. A., Pérez-Ángel, G., and Nahmad-Molinari, Y.: Runout transition and

clustering instability observed in binary-mixture avalanche deposits, Granular Matter, 22, 30, 10.1007/s10035-019-0989-

0, 2020.

Bowman, E. T. and Take, W. A.: The runout of chalk cliff collapses in England and France—case studies and physical model

experiments, Landslides, 12, 225-239, 10.1007/s10346-014-0472-2, 2015.

405   Charrière, M., Humair, F., Froese, C., Jaboyedoff, M., Pedrazzini, A., and Longchamp, C.: From the source area to the deposit:

Collapse, fragmentation, and propagation of the Frank Slide, GSA Bulletin, 128, 332-351, 10.1130/B31243.1, 2016.

19

Cole, P. D., Calder, E. S., Sparks, R. S. J., Clarke, A. B., Druitt, T. H., Young, S. R., Herd, R. A., Harford, C. L., and Norton, G. E.: Deposits from dome-collapse and fountain-collapse pyroclastic flows at Soufrière Hills Volcano, Montserrat, Geological Society, London, Memoirs, 21, 231, 10.1144/GSL.MEM.2002.021.01.11, 2002.

410 Crosta, G. B., Blasio, F. V. D., Locatelli, M., Imposimato, S., and Roddeman, D.: Landslides falling onto a shallow erodible substrate or water layer: an experimental and numerical approach, IOP Conference Series: Earth and Environmental Science, 10.1088/1755-1315/26/1/012004, 2015.

Crosta, G. B., Blasio, F. V. D., Caro, M. D., Volpi, G., Imposimato, S., and Roddeman, D.: Modes of propagation and deposition of granular flows onto an erodible substrate: experimental, analytical, and numerical study, Landslides, 14, 47–68,
415 https://doi.org/10.1007/s10346-016-0697-3, 2017.

Dasgupta, P. and Manna, P.: Geometrical mechanism of inverse grading in grain-flow deposits: An experimental revelation, Earth-Science Reviews, 104, 186-198, https://doi.org/10.1016/j.earscirev.2010.10.002, 2011.

Deganutti, A. M.: The Hypermobility of Rock Avalanches, Dipartimento di Geoscienze, Università degli Studi di Padova, 2008.

Delannay, R., Valance, A., Roche4, O., and Richard, P.: Granular and particle-laden flows: from laboratory experiments to
420 field observations, Journal of Physics D: Applied Physic, 50 (5), pp.40. 10.1088, hal-univ-rennes1.archives-ouvertes.fr/hal-01481019, 2017.

Duan, Z., Cheng, W.-C., Peng, J.-B., Rahman, M. M., and Tang, H.: Interactions of landslide deposit with terrace sediments: Perspectives from velocity of deposit movement and apparent friction angle, Engineering Geology, 280, 105913, https://doi.org/10.1016/j.enggeo.2020.105913, 2021.

425 Duan, Z., Cheng, W.-C., Peng, J.-B., Wang, Q.-Y., and Chen, W.: Investigation into the triggering mechanism of loess landslides in the south Jingyang platform, Shaanxi province, Bulletin of Engineering Geology and the Environment, 78, 4919-4930, 10.1007/s10064-018-01432-8, 2019.

Duan, Z., Wu, Y. B., Tang, H., Ma, J. Q., and Zhu, X. H.: An Analysis of Factors Affecting Flowslide Deposit Morphology Using Taguchi Method, Advances in Civil Engineering, 2020, 1-14, 10.1155/2020/8844722, 2020.

430 Dufresne, A.: Granular flow experiments on the interaction with stationary runout path materials and comparison to rock avalanche events, Earth surface processes and landforms, 37, 1527-1541, 2012.

Dufresne, A.: Rock Avalanche Sedimentology—Recent Progress, Advancing Culture of Living with Landslides, Cham, 2017//, 117-122,

Dufresne, A. and Dunning, S. A.: Process dependence of grain size distributions in rock avalanche deposits, Landslides, 14,
435 1555-1563, 10.1007/s10346-017-0806-y, 2017.

Dufresne, A., Bösmeier, A., and Prager, C.: Sedimentology of rock avalanche deposits – Case study and review, Earth-Science Reviews, 163, 234-259, 10.1016/j.earscirev.2016.10.002, 2016.

Dufresne, A., Zernack, A., Bernard, K., Thouret, J.-C., and Roverato, M.: Sedimentology of Volcanic Debris Avalanche

Deposits, in: Volcanic Debris Avalanches: From Collapse to Hazard, edited by: Roverato, M., Dufresne, A., and Procter, J.,

440   Springer International Publishing, Cham, 175-210, 10.1007/978-3-030-57411-6_8, 2021.

Fan, X. y., Tian, S. j., and Zhang, Y. y.: Mass-front velocity of dry granular flows influenced by the angle of the slope to the

runout plane and particle size gradation, Journal of Mountain Science, 13, 234-245, 10.1007/s11629-014-3396-3, 2016.

Felix, G. and Thomas, N.: Evidence of two effects in the size segregation process in dry granular media, Phys Rev E Stat

Nonlin Soft Matter Phys, 70, 051307, 10.1103/PhysRevE.70.051307, 2004.

445   Fisher, R. V. and Heiken, G.: Mt. Pelée, martinique: may 8 and 20, 1902, pyroclastic flows and surges, Journal of Volcanology

and Geothermal Research, 13, 339-371, https://doi.org/10.1016/0377-0273(82)90056-7, 1982.

Getahun, E., Qi, S.-w., Guo, S.-f., Zou, Y., and Liang, N.: Characteristics of grain size distribution and the shear strength

analysis of Chenjiaba long runout coseismic landslide, Journal of Mountain Science, 16, 2110-2125, 10.1007/s11629-019-

5535-3, 2019.

450   Glicken, H., Survey, U. S. G. (Ed.): Rockslide-debris avalanche of May 18, 1980, Mount St. Helens Volcano, Washington,

Open-File Report, 98 pp., 10.3133/ofr96677, 1996.

Goujon, C., Thomas, N., and Dalloz-Dubrujeaud, B.: Monodisperse dry granular flows oninclined planes: Role of roughness,

The European Physical Journal E, 11, 147-157, 10.1140/epje/i2003-10012-0, 2003.

Gray, J. M. N. T. and Hutter, K.: Pattern formation in granular avalanches, Continuum Mechanics and Thermodynamics, 9,

455   341-345, 10.1007/s001610050075, 1997.

Huang, R. Q. and Liu, W. H.: In-situ test study of characteristics of rolling rock blocks based on orthogonal design, Chinese

Journal of Rock Mechanics Engineering Geology(in Chinese), 28, 882-891, 2009.

Hungr, O.: ROCK AVALANCHE OCCURRENCE, PROCESS AND MODELLING, Landslides from Massive Rock Slope

Failure, Dordrecht, 2006//, 243-266,

460   Ji, Z.-M., Chen, Z.-J., Niu, Q.-H., Wang, T.-J., Song, H., and Wang, T.-H.: Laboratory study on the influencing factors and

their control for the coefficient of restitution during rockfall impacts, Landslides, 16, 1939-1963, 10.1007/s10346-019-

01183-x, 2019.

Johnson, C. G., Kokelaar, B. P., Iverson, R. M., Logan, M., LaHusen, R. G., and Gray, J. M. N. T.: Grain-size segregation and

levee   formation   in   geophysical   mass   flows,   Journal   of   Geophysical   Research: Earth   Surface,   117,

465   https://doi.org/10.1029/2011JF002185, 2012.

Jomelli, V. and Bertran, P.: Wet snow avalanche deposits in the french alps: structure and sedimentology, Geografiska Annaler:

Series A, Physical Geography, 83, 15-28, 10.1111/j.0435-3676.2001.00141.x, 2001.

Li, H., Duan, Z., Wu, Y., Dong, C., and Zhao, F.: The Motion and Range of Landslides According to Their Height, Frontiers

in Earth Science, 9, 811, 2021.

470   Li, L. P., Sun, S. Q., Li, S. C., Zhang, Q. Q., Hu, C., and Shi, S. S.: Coefficient of restitution and kinetic energy loss of rockfall

impacts, KSCE Journal of Civil Engineering, 20, 2297-2307, 10.1007/s12205-015-0221-7, 2015.

Lucas, A. and Mangeney, A.: Mobility and topographic effects for large Valles Marineris landslides on Mars, GEOPHYSICAL RESEARCH LETTERS, 34, L10201, https://doi.org/10.1029/2007GL029835, 2007.

Makris, S., Manzella, I., Cole, P., and Roverato, M.: Grain size distribution and sedimentology in volcanic mass-wasting flows:
475   implications for propagation and mobility, International Journal of Earth Sciences, 109, 2679-2695, 10.1007/s00531-020-01907-8, 2020.

Mangeney, A., Roche, O., Hungr, O., Mangold, N., Faccanoni, G., and Lucas, A.: Erosion and mobility in granular collapse over sloping beds, Journal of Geophysical Research, 115, 10.1029/2009jf001462, 2010.

Mangold, N., Mangeney, A., Migeon, V., Ansan, V., Lucas, A., Baratoux, D., and Bouchut, F.: Sinuous gullies on Mars:
480   Frequency, distribution, and implications for flow properties, Journal of Geophysical Research, 115, 10.1029/2009je003540, 2010.

Manzella, I. and Labiouse, V.: Flow experiments with gravel and blocks at small scale to investigate parameters and mechanisms involved in rock avalanches, Engineering Geology, 109, 146-158, 2009.

Manzella, I. and Labiouse, V.: Empirical and analytical analyses of laboratory granular flows to investigate rock avalanche
485   propagation, Landslides, 10, 23-26, 10.1007/s10346-011-0313-5, 2013a.

Manzella, I. and Labiouse, V.: Empirical and analytical analyses of laboratory granular flows to investigate rock avalanche propagation, Landslides, 10, 23-26, 10.1007/s10346-011-0313-5, 2013b.

McDougall, S.: 2014 Canadian Geotechnical Colloquium: Landslide runout analysis — current practice and challenges, Canadian Geotechnical Journal, 54, 605-620, 10.1139/cgj-2016-0104, 2016.

490 Moreiras, S. M.: The Plata Rock Avalanche: Deciphering the Occurrence of This Huge Collapse in a Glacial Valley of the Central Andes (33° S), 8, 10.3389/feart.2020.00267, 2020.

Pánek, T., Hradecký, J., Smolková, V., and Šilhán, K.: Gigantic low-gradient landslides in the northern periphery of the Crimean Mountains (Ukraine), Geomorphology, 95, 449-473, https://doi.org/10.1016/j.geomorph.2007.07.007, 2008.

Phillips, J. C., Hogg, A. J., Kerswell, R. R., and Thomas, N. H.: Enhanced mobility of granular mixtures of fine and coarse
495   particles, Earth and Planetary Science Letters, 246, 466-480, https://doi.org/10.1016/j.epsl.2006.04.007, 2006.

Reznichenko, N. V., Davies, T. R. H., and Alexander, D. J.: Effects of rock avalanches on glacier behaviour and moraine formation, Geomorphology, 132, 327-338, https://doi.org/10.1016/j.geomorph.2011.05.019, 2011.

Schwarzkopf, L. M., Schmincke, H.-U., and Cronin, S. J.: A conceptual model for block-and-ash flow basal avalanche transport and deposition, based on deposit architecture of 1998 and 1994 Merapi flows, Journal of Volcanology and Geothermal
500   Research, 139, 117-134, https://doi.org/10.1016/j.jvolgeores.2004.06.012, 2005.

Shea, T. and van Wyk de Vries, B.: Structural analysis and analogue modeling of the kinematics and dynamics of rockslide avalanches, Geosphere, 4, 657-686, 10.1130/GES00131.1, 2008.

Shugar, D. H. and Clague, J. J.: The sedimentology and geomorphology of rock avalanche deposits on glaciers, Sedimentology, 58, 1762-1783, https://doi.org/10.1111/j.1365-3091.2011.01238.x, 2011.

505   Ui, T., Kawachi, S., and Neall, V. E.: Fragmentation of debris avalanche material during flowage — Evidence from the Pungarehu Formation, Mount Egmont, New Zealand, Journal of Volcanology and Geothermal Research, 27, 255-264, https://doi.org/10.1016/0377-0273(86)90016-8, 1986.

Voight, B. and Pariseau, W. G.: Rockslides and Avalanches: An Introduction, in: Developments in Geotechnical Engineering, edited by: Voight, B., Elsevier, 1-67, https://doi.org/10.1016/B978-0-444-41507-3.50008-8, 1978.

510   Wang, Y.-F., Cheng, Q.-G., Shi, A.-W., Yuan, Y.-Q., Yin, B.-M., and Qiu, Y.-H.: Sedimentary deformation structures in the Nyixoi Chongco rock avalanche: implications on rock avalanche transport mechanisms, Landslides, 16, 523-532, 10.1007/s10346-018-1117-7, 2019.

Wang, Y., Cheng, Q., Lin, Q., Li, K., and Shi, A.: Observations on the sedimentary structure of prehistoric rock avalanches on the Tibetan Plateau, China, Earth Science Frontiers (in Chinese), 28, 106-124, 2021.

515   Wang, Y., Jiang, W., Cheng, S., Song, P., and Mao, C.: Effects of the impact angle on the coefficient of restitution in rockfall analysis based on a medium-scale laboratory test, Nat. Hazards Earth Syst. Sci., 18, 3045-3061, 10.5194/nhess-18-3045-2018, 2018.

Yang, Q., Cai, F., Ugai, K., Yamada, M., Su, Z., Ahmed, A., Huang, R., and Xu, Q.: Some factors affecting mass-front velocity of rapid dry granular flows in a large flume, Engineering Geology, 122, 249-260, 520   https://doi.org/10.1016/j.enggeo.2011.06.006, 2011.

Zeng, Q., Wei, R., McSaveney, M., Ma, F., Yuan, G., and Liao, L.: From surface morphologies to inner structures: insights into hypermobility of the Nixu rock avalanche, southern Tibet, China, Landslides, 10.1007/s10346-020-01503-6, 2020.

Zhang, G., Tang, H., Xiang, X., Murat, K., and Wu, J.: Theoretical study of rockfall impacts based on logistic curves, International Journal of Rock Mechanics and Mining Sciences, 78, 133-143, https://doi.org/10.1016/j.ijrmms.2015.06.001, 525   2015.

Zhang, M., Wu, L., Zhang, J., and Li, L.: The 2009 Jiweishan rock avalanche, Wulong, China: deposit characteristics and implications for its fragmentation, Landslides, 16, 893-906, 10.1007/s10346-019-01142-6, 2019.

Zhao, B., Zhao, X., Zeng, L., Wang, S., and Du, Y.: The mechanisms of complex morphological features of a prehistorical landslide on the eastern margin of the Qinghai-Tibetan Plateau, Bulletin of Engineering Geology and the Environment, 80, 530   3423-3437, 10.1007/s10064-021-02114-8, 2021.